

Nuclear applications of ANL-Osaka amplitudes: pion photo-productions on deuteron

S. X. Nakamura,¹ H. Kamano,² T.-S. H. Lee,³ and T. Sato^{2,4}

¹*Laboratório de Física Teórica e Computacional - LFTC, Universidade Cruzeiro do Sul, São Paulo, SP 01506-000, Brazil*

²*Research Center for Nuclear Physics, Osaka University, Ibaraki, Osaka 567-0047, Japan*

³*Physics Division, Argonne National Laboratory, Argonne, Illinois 60439, USA*

⁴*J-PARC Branch, KEK Theory Center, IPNS, KEK, Tokai, Ibaraki 319-1106, Japan*

Abstract

The Argonne National Laboratory-Osaka University (ANL-Osaka) amplitudes (<http://www.phy.anl.gov/theory/research/anl-osaka-pwa/>) are applied to study pion photo-production reactions on the deuteron target. Within the multiple scattering formulation, we predict the cross sections of $d(\gamma, \pi)NN$ in the nucleon resonance region. The calculations include the impulse term and the final-state interaction (FSI) terms due to pion-exchange and nucleon-exchange. We show that the off-shell effects, calculated from the meson-exchange mechanisms, on the propagations of the exchanged nucleon and pion are significant in determining the reaction amplitudes. The FSI effects on the predicted cross sections are found to be important at energies near the $\Delta(1232)$ resonance, and are still significant at higher energies. The results are in good agreement with most of the available data of $d(\gamma, \pi^0)np$ and $d(\gamma, \pi^-)pp$ reactions.

PACS numbers: 11.80.La, 13.60.Le, 13.88.+e, 14.20.Gk

I. INTRODUCTION

The developments of dynamical models for πN and γN reactions were motivated by the success of the meson-exchange models [2] for the NN interactions and the earlier attempts [3] to relate the isobar models of nucleon resonances to the predictions of constituent quark models [4]. Within the formulation given in Refs. [5, 6], the development of dynamical models of πN and γN reactions has two main objectives:

1. Develop interpretations of the nucleon resonances (N^*) within the framework that the excitations of the nucleon can be described in terms of bare baryon states and meson-exchange interactions. With the parameters determined by fitting the data of πN and γN reactions up to the invariant mass $W = 2$ GeV, the poles and residues of nucleon resonances are extracted by performing analytic continuations of the partial-wave amplitudes predicted within the constructed model to the complex energy-plane.
2. Apply the constructed dynamical model to investigate the production and propagation of mesons and nucleon resonances in nuclei, which are crucial for analyzing data from experiments on nuclear targets in the nucleon resonance region, such as the recent experiments on the neutrino oscillations [7].

With the efforts reported in Refs. [8–20], we have achieved the first objective, and the resulting Argonne National Laboratory-Osaka University (ANL-Osaka) amplitudes has now become available [1] to public. In this paper, we will take a step toward reaching the second objective by applying the constructed dynamical coupled-channel model (ANL-Osaka model) presented in Ref. [19, 20] to investigate pion photo-production on the simplest nucleus, the deuteron (d). We will focus on the $d(\gamma, \pi)NN$ reactions for the following reason. An uncertainty in the construction of the ANL-Osaka model was in the determination of the isospin structure of the nucleon resonances by fitting the available data of $\gamma n \rightarrow \pi^- p$ which were extracted from the $d(\gamma, \pi^-)pp$ data with some procedures to select the $\gamma n \rightarrow \pi^- p$ events. Furthermore, $\gamma n \rightarrow \pi^0 n$ data included in our previous fit were rather scarce.¹ We therefore need to examine whether our predictions of $d(\gamma, \pi)NN$ will be in agreement with the original data of $d(\gamma, \pi^-)pp$ and $d(\gamma, \pi^0)pn$.

One of the important features of the ANL-Osaka model is that the amplitudes are generated from an energy *independent* Hamiltonian which can be included in the conventional Hamiltonian formulation for developing many-body descriptions of nuclear reactions. This is achieved by using a unitary transformation method [5, 27] to derive hadron-hadron interactions from relativistic quantum field theory with meson and baryon degrees of freedom. This feature allows us to use rigorously the well-established multiple-scattering formulation [28] to develop a reaction model for $d(\gamma, \pi)NN$ reactions. For our limited purpose here, we follow the previous investigations [25, 26, 29–33] to only include the single scattering (impulse) amplitudes and the double scattering amplitudes due to pion-exchange and nucleon-exchange mechanisms. The exchanges of unstable particles ρ , σ and $\Delta(1232)$, which can be generated from the ANL-Osaka model, are more difficult to calculate and are neglected in this work for simplicity.

Thus our task is to develop formula for calculating the amplitudes illustrated in Fig. 1. The $\gamma N \rightarrow \pi N$ and $\pi N \rightarrow \pi N$ amplitudes for evaluating the pion re-scattering term of

¹ For determining the isospin structure of nucleon resonances, $\gamma p \rightarrow \pi^0 p, \pi^+ n$ data and either of $\gamma n \rightarrow \pi^- p$ or $\gamma n \rightarrow \pi^0 n$ data are needed in the fit if the data are of very high accuracy. This is however not the case, thus the fits including both of the neutron data may be needed to reduce the uncertainty.

Fig. 1(c) can be generated from the ANL-Osaka model. The initial deuteron wave function and the $NN \rightarrow NN$ amplitudes in Fig. 1(b) can be generated from any of the available high-precision NN potentials. To be consistent with the meson-exchange mechanisms of the ANL-Osaka model, we choose the CD-Bonn potential [34]. There are two important issues in practical calculations of the matrix elements of these mechanisms, as discussed well in the earlier investigations [35, 36] of the multiple scattering of hadrons from nuclei within the Hamiltonian formulation. First, we need to define a Lorentz boost transformation to relate the $\gamma N \rightarrow \pi N$, $\pi N \rightarrow \pi N$ and $NN \rightarrow NN$ amplitudes in Fig. 1 in the photon-deuteron laboratory frame to those in the two-body center of mass (CM) frame where the two-body amplitudes are generated from Hamiltonian by solving scattering equations in partial-wave representation. In particular, the spin rotations must be taken into account relativistically for investigating polarization observables. Here we follow the method of relativistic quantum mechanics, as detailed in Ref. [37–39]. The second issue is that the resulting FSI amplitudes will include loop-integrations over the off-energy-shell matrix elements of the two-body amplitudes in Fig. 1. Thus it is necessary to introduce an approximation to choose the collision energies in generating these two-body off-shell matrix elements. Here we will use an approach which accounts for the energy shared by the spectator nucleon and pion in Fig. 1.

The organization of the rest of this paper is as follows. In Sec. II, we present formulas for calculating the amplitudes of the impulse term [Fig. 1.(a)], nucleon re-scattering (N -exchange) term [Fig. 1.(b)], and pion re-scattering (π -exchange) term [Fig. 1.(c)]. The results for comparing our predictions with the available data of $d(\gamma, \pi^0)pn$ and $d(\gamma, \pi^0)pp$, and for examining the importance of FSI and off-shell effects will be given in Sec. III. A summary is given in Sec. IV.

II. FORMULATION

In this section, we describe the theoretical formulation used in our investigation of $d(\gamma, \pi)NN$ reactions. All of the formulas for calculations are presented with the normalizations: $\langle \mathbf{k}' | \mathbf{k} \rangle = \delta^{(3)}(\mathbf{k}' - \mathbf{k})$ for plane-wave states and $\langle \Phi_d | \Phi_d \rangle = 1$ for bound states.

A. Model Hamiltonian with meson and baryon degrees of freedom

Our starting point is the following many-body Hamiltonian

$$H = H_0 + \frac{1}{2} \sum_{i \neq j} V_{NN,NN}(i, j) + \sum_i h_{\text{AO}}^I(i), \quad (1)$$

where H_0 is the free Hamiltonian for all particles in the considered processes, $V_{NN,NN}(i, j)$ is a nucleon-nucleon potential between the nucleons i and j , and

$$h_{\text{AO}}^I(i) = \sum_{c, c'} v_{c, c'}(i) + \sum_{N^*} \sum_c [\Gamma_{N^*, c}(i) + \Gamma_{N^*, c}^\dagger(i)], \quad (2)$$

is the interaction Hamiltonian of the ANL-Osaka (AO) model. The channels included are $c, c' = \gamma N, \pi N, \eta N, K\Lambda, K\Sigma$ and $\pi\pi N$ with resonant $\pi\Delta, \rho N$, and σN components. The energy independent meson-exchange potentials $v_{c, c'}$ are derived from phenomenological Lagrangians by using the unitary transformation method [5, 27]. The vertex interaction $\Gamma_{N^*, c}$

defines the formation of a bare N^* state from a channel c . The parameters of the Hamiltonian h_{AO}^I have been determined in Refs. [19, 20] by fitting about 26,000 data points of the πN and γN reactions up to the invariant mass $W \simeq 2$ GeV.

Here we mention that the model Hamiltonian defined above is a very significant extension of the Hamiltonian developed in Refs. [40, 41] where only π , N , and Δ degrees of freedom are included. It can be used to investigate π , η , and two-pion production reactions on nuclei in the nucleon resonance region. The first attempt in this direction was made to investigate the $d(\gamma, \eta)pn$ reaction in the context of extracting the low-energy ηN scattering parameters [42]. Here we focus on the pion photo-production on the deuteron to test our predictions.

B. Scattering amplitudes for $d(\gamma, \pi)NN$ reactions

Starting with the scattering T -matrix given by the Hamiltonian Eq. (1), it is straightforward to follow the well-developed procedures [28] to obtain a multiple scattering formulation of the $d(\gamma, \pi)NN$ reactions. Following the previous investigations [25, 26, 29, 33], we will only keep the single-scattering (impulse) terms and the double scattering terms with πNN intermediate states. The T -matrix operator for the $d(\gamma, \pi)NN$ reactions can then be written as

$$T(E) = \sum_i \tau_{\pi N_i, \gamma N_i}(E) + \sum_{i \neq j} \tau_{N_i N_j, N_i N_j}(E) \frac{|\pi N_i N_j\rangle \langle \pi N_i N_j|}{E - H_0 + i\epsilon} \tau_{\pi N_i, \gamma N_i}(E) \\ + \sum_{i \neq j} \tau_{\pi N_j, \pi N_j}(E) \frac{|\pi N_i N_j\rangle \langle \pi N_i N_j|}{E - H_0 + i\epsilon} \tau_{\pi N_i, \gamma N_i}(E), \quad (3)$$

where E is the total energy of the γd system, $\tau_{\alpha N_i, \beta N_i}(E)$ is a scattering operator associated with the i -th nucleon in the deuteron. Note that the matrix elements of $\tau_{\alpha N_i, \beta N_i}(E)$ are determined by the total Hamiltonian Eq. (1) and cannot be calculated exactly. Therefore, we adopt the spectator approximation [35, 36] as

$$\tau_{\alpha, N_i, \beta N_i}(E) \sim t_{\alpha, N_i, \beta N_i}(E - E_{\text{spectator}}), \quad (4)$$

where $t_{\alpha, N_i, \beta N_i}(E')$ is the two-body scattering operator in free space, and $E_{\text{spectator}}$ is the energy of the spectator of the two-body scattering in the γNN or πNN three-particle states, as seen in Fig. 1. The resulting T -matrix operator is consistent with that of the Faddeev framework up to and including the double scattering terms, as has been also discussed in Ref. [42].

To proceed further, we need to define the matrix elements of the scattering operator $t_{c, c'}(W)$ with an invariant mass W . Within the ANL-Osaka model, these matrix elements are generated in the two-body CM frame by solving the following coupled-channel equations in each partial wave:

$$\langle k | t_{c, c'}(W) | k' \rangle = \langle k | V_{c, c'}(W) | k' \rangle \\ + \sum_{c''} \int k''^2 dk'' \frac{\langle k | V_{c, c''}(W) | k'' \rangle \langle k'' | t_{c'', c'}(W) | k' \rangle}{W - E_{c'', 1}(k'') - E_{c'', 2}(k'') - \Sigma_{c''}(k'', W) + i\epsilon}, \quad (5)$$

where k , k' and k'' are the momenta in the CM frame, $E_{c, i}(k) = \sqrt{m_{c, i}^2 + k^2}$ is the energy of a particle i in a channel c with the mass $m_{c, i}$, $c, c', c'' = \pi N, \eta N, \pi \Delta, \rho N, \sigma N, K \Lambda, K \Sigma$ are the

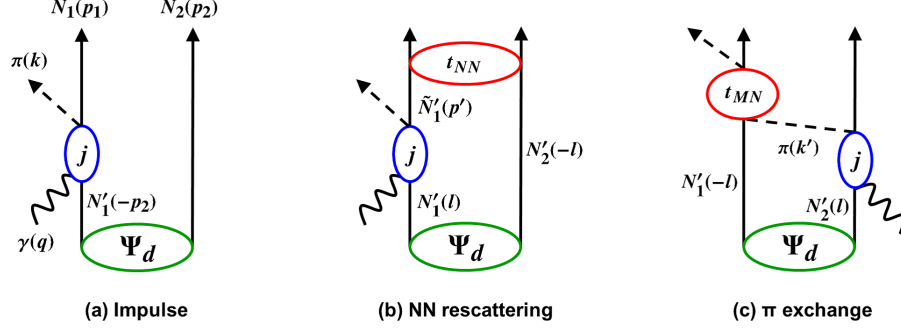


FIG. 1. Diagrammatic representation of reaction mechanisms considered in this work for $d(\gamma, \pi)NN$: (left) impulse, (center) NN rescattering (N -exchange), (right) πN rescattering (π -exchange) mechanisms.

considered channels, and $c' = \gamma N$ channel is included perturbatively; $\Sigma_{c'}$ is the self-energy for the unstable channels $c'' = \pi\Delta, \rho N, \sigma N$, and is zero for the other stable channels. The driving term is

$$V_{c,c'}(W) = v_{c,c'} + \sum_{N^*} \Gamma_{N^*,c}^\dagger \frac{1}{W - M_{N^*}} \Gamma_{N^*,c'} + Z(W), \quad (6)$$

where M_{N^*} is the bare mass of an excited nucleon state N^* ; $Z(W)$ is a particle-exchange Z-diagram in which a $\pi\pi N$ channel is included. Note that the initial and final states of each matrix element in Eq. (5) can be on-energy-shell [$W = E_{c,1}(k) + E_{c,2}(k) = E_{c',1}(k') + E_{c',2}(k')$] or off-energy-shell [$W \neq E_{c,1}(k) + E_{c,2}(k) \neq E_{c',1}(k') + E_{c',2}(k')$] within the Hamiltonian formulation.

By using Eqs. (3) and (4) and the momenta defined in Fig. 1, the Lorentz invariant scattering amplitude of $d(\gamma, \pi)NN$ can then be written as

$$M_{f,i}(E) = \sqrt{\frac{(2E_\pi(\mathbf{k}))E_N(\mathbf{p}_1)E_N(\mathbf{p}_2)}{m_N^2}} \times \left(t_{f,i}^{\text{imp}}(E) + t_{f,i}^{N\text{-exc}}(E) + t_{f,i}^{\pi\text{-exc}}(E) + \{\text{exchange terms}\} \right) \sqrt{(2\omega)(2E_d(\mathbf{p}_d))}, \quad (7)$$

where the sub-indices f and i stand for the final state $\langle \pi(\mathbf{k}, t_\pi) N_1(\mathbf{p}_1, s_1, t_1), N_2(\mathbf{p}_2, s_2, t_2) |$, and the initial state $|\gamma(\mathbf{q}, \lambda), \Psi_d(s_d)\rangle$, respectively, $\omega = |\mathbf{q}|$ is the photon energy, and for the

laboratory frame,

$$t_{f,i}^{\text{imp}} = \sqrt{2} \sum_{s'_1, t'_1} \langle \pi(\mathbf{k}, t_\pi) N_1(\mathbf{p}_1, s_1, t_1) | t_{\pi N, \gamma N}(M_{\pi N_1}) | \gamma(\mathbf{q}, \lambda) N'_1(-\mathbf{p}_2, s'_1, t'_1) \rangle \\ \times \langle N'_1(-\mathbf{p}_2, s'_1, t'_1) N_2(\mathbf{p}_2, s_2, t_2) | \Psi_d(s_d) \rangle , \quad (8)$$

$$t_{f,i}^{N\text{-exc}} = \sqrt{2} \sum_{s'_1, \tilde{s}'_1, s'_2, t'_1} \int d\mathbf{l} \\ \times \langle N_1(\mathbf{p}_1, s_1, t_1) N_2(\mathbf{p}_2, s_2, t_2) | t_{NN, NN}(M_{N_1 N_2}) | \tilde{N}'_1(\mathbf{q} - \mathbf{k} + \mathbf{l}, \tilde{s}'_1, t_1) N'_2(-\mathbf{l}, s'_2, t_2) \rangle \\ \times \frac{\langle \pi(\mathbf{k}, t_\pi) \tilde{N}'_1(\mathbf{q} - \mathbf{k} + \mathbf{l}, \tilde{s}'_1, t_1) | t_{\pi N, \gamma N}(W) | \gamma(\mathbf{q}, \lambda) N'_1(\mathbf{l}, s'_1, t'_1) \rangle}{E - E_N(\mathbf{q} - \mathbf{k} + \mathbf{l}) - E_N(-\mathbf{l}) - E_\pi(\mathbf{k}) + i\epsilon} \\ \times \langle N'_1(\mathbf{l}, s'_1, t'_1) N'_2(-\mathbf{l}, s'_2, t_2) | \Psi_d(s_d) \rangle , \quad (9)$$

$$t_{f,i}^{\pi\text{-exc}} = \sqrt{2} \sum_{s'_1, s'_2} \sum_{t'_1, t'_2, t'_\pi} \int d\mathbf{l} \langle \pi(\mathbf{k}, t_\pi) N_1(\mathbf{p}_1, s_1, t_1) | t_{\pi N, \pi N}(M_{\pi N_1}) | \pi(\mathbf{q} - \mathbf{p}_2 + \mathbf{l}, t'_\pi) N'_1(-\mathbf{l}, s'_1, t'_1) \rangle \\ \times \frac{\langle \pi(\mathbf{q} - \mathbf{p}_2 + \mathbf{l}, t'_\pi) N_2(\mathbf{p}_2, s_2, t_2) | t_{\pi N, \gamma N}(W) | \gamma(\mathbf{q}, \lambda) N'_2(\mathbf{l}, s'_2, t'_2) \rangle}{E - E_N(\mathbf{p}_2) - E_N(-\mathbf{l}) - E_\pi(\mathbf{q} - \mathbf{p}_2 + \mathbf{l}) + i\epsilon} \\ \times \langle N'_1(-\mathbf{l}, s'_1, t'_1) N'_2(\mathbf{l}, s'_2, t'_2) | \Psi_d(s_d) \rangle . \quad (10)$$

The exchange terms in Eq. (7) can be obtained from Eqs. (8)-(10) by flipping the overall sign and interchanging all subscripts 1 and 2 for the nucleons in the intermediate and final πNN states. Here, the deuteron state with spin projection s_d is denoted as $|\Psi_d(s_d)\rangle$; $|N(\mathbf{p}, s, t)\rangle$ the nucleon state with momentum \mathbf{p} and spin and isospin projections s and t ; $|\gamma(\mathbf{q}, \lambda)\rangle$ the photon state with momentum \mathbf{q} and polarization λ ; $|\pi(\mathbf{k}, t_\pi)\rangle$ the pion state with momentum \mathbf{k} and the isospin projection t_π . The total energy in the laboratory frame, E , is given by $E = \omega + m_d$ where m_d is the deuteron mass. The invariant masses for the matrix elements of the two-body subprocesses are calculated according to the momentum variables specified in Fig. 1 and $E - E_{\text{spectator}}$ of the spectator approximation defined by Eq. (4):

$$M_{\pi N_1} = \sqrt{[E_\pi(\mathbf{k}) + E_N(\mathbf{p}_1)]^2 - (\mathbf{k} + \mathbf{p}_1)^2} , \quad (11)$$

$$M_{N_1 N_2} = \sqrt{[E_N(\mathbf{p}_1) + E_N(\mathbf{p}_2)]^2 - (\mathbf{p}_1 + \mathbf{p}_2)^2} , \quad (12)$$

$$W = \sqrt{[E - E_N(-\mathbf{l})]^2 - (\mathbf{l} + \mathbf{q})^2} . \quad (13)$$

To be consistent with the chosen CD-Bonn NN potential [34] for generating the NN scattering amplitudes and the deuteron bound state, the two-nucleon energy in the propagator of the nucleon re-scattering amplitude $t_{NN, NN}$ in Eq. (9), is calculated with a non-relativistic approximation

$$E_N(\mathbf{q} - \mathbf{k} + \mathbf{l}) + E_N(-\mathbf{l}) \sim \sqrt{(2m_N)^2 + (\mathbf{q} - \mathbf{k})^2} + \frac{(\mathbf{q}/2 - \mathbf{k}/2 + \mathbf{l})^2}{m_N} . \quad (14)$$

The amplitudes $\langle \pi N | t_{\pi N, \gamma N} | \gamma N' \rangle$ of the pion photoproduction and $\langle \pi N | t_{\pi N, \pi N} | \pi' N' \rangle$ of the pion-nucleon scattering in Eqs. (8)-(10) are first generated from the ANL-Osaka model by solving the coupled-channel equation of Eq. (5) in the two-body CM frame. The resulting matrix elements are then boosted to the considered γ -deuteron frame. Here we follow the approach of Ref. [37] based on the instant form of relativistic quantum mechanics [39]. The same frame-transformation procedure is also needed to calculate the matrix element

$\langle NN|t_{NN,NN}|NN\rangle$ of NN scattering in Eq. (9). The formulas for calculating these matrix elements in the γ -deuteron frame are given in Appendix A.

Here we note an important difference between our dynamical model approach and the approach of Refs. [25, 26]. In the loop-integrations of Eqs. (9) and (10), the two-body matrix elements can be off-energy-shell and are calculated exactly from the ANL-Osaka model and the CD-Bonn potential as explained above. The equations for calculating FSI in Refs. [25, 26] are similar to our expressions, but the two-body matrix elements are taken as their on-shell values and are taken out of the loop-integrations. For $NN \rightarrow NN$, they include a monopole form factor of Ref. [31] to account for the off-shell effect. These simplifications greatly reduce the computation task. We will examine the on-shell approximation within our formulation in Sec. III.

C. Cross section formula

The reaction cross section for $\gamma(\mathbf{q}) + d(\mathbf{p}_d) \rightarrow \pi(\mathbf{k}) + N_1(\mathbf{p}_1) + N_2(\mathbf{p}_2)$ is defined by

$$d\sigma = \frac{(2\pi)^4}{|\mathbf{v}_{rel}|} \delta^{(3)}(\mathbf{p}_d + \mathbf{q} - \mathbf{p}_1 - \mathbf{p}_2 - \mathbf{k}) \delta(E_d(\mathbf{p}_d) + \omega - E_N(\mathbf{p}_1) - E_N(\mathbf{p}_2) - E_\pi(\mathbf{k})) \\ \times d\mathbf{p}_1 d\mathbf{p}_2 d\mathbf{k} \left[\frac{m_N}{E_N(\mathbf{p}_1)} \frac{m_N}{E_N(\mathbf{p}_2)} \frac{1}{2E_\pi(\mathbf{k})} \right] |M_{f,i}(E)|^2 \left[\frac{1}{2E_d(\mathbf{p}_d)} \frac{1}{2\omega} \right], \quad (15)$$

where \mathbf{v}_{rel} is the relative velocity of the initial γ - d system, and the Lorentz invariant amplitude $M_{f,i}(E)$ has been defined by Eqs. (7)-(10). The unpolarized differential cross section with respect to the pion emission angle in the laboratory frame ($\mathbf{p}_d = 0$) derived from Eq. (15) can be written as

$$\frac{d\sigma}{d\Omega} \equiv \frac{d\sigma}{d\Omega_{\mathbf{k}}} = \frac{1}{6} \sum_{\lambda, s_d} \frac{d\sigma(\lambda, s_d)}{d\Omega_{\mathbf{k}}}, \quad (16)$$

where λ is the photon polarization, s_d is the z -component of the deuteron spin, and

$$\frac{d\sigma(\lambda, s_d)}{d\Omega_{\mathbf{k}}} = \int dM_{NN} \frac{d\sigma(\lambda, s_d)}{d\Omega_{\mathbf{k}} dM_{NN}}, \quad (17)$$

with

$$\frac{d\sigma(\lambda, s_d)}{d\Omega_{\mathbf{k}} dM_{NN}} = \sum_{s_1, s_2} \frac{(2\pi)^4}{4\omega} \frac{1}{2E_d(\mathbf{p}_d)} \int d\Omega_{\mathbf{p}_{NN}} \frac{p_{NN} k^2 m_N^2}{|kE - \mathbf{q} \cdot \hat{k} E_\pi(\mathbf{k})|} |M_{f,i}(E)|^2. \quad (18)$$

Here $E = m_d + \omega$ is the total energy in the laboratory frame, \mathbf{p}_{NN} the momentum of N_1 in the $N_1 N_2$ CM frame, and M_{NN} the invariant mass of the two nucleons in the final πNN state. The magnitudes of the momenta are simply denoted, for example, by $k \equiv |\mathbf{k}|$, and $\hat{k} \equiv \mathbf{k}/|\mathbf{k}|$. To evaluate the Lorentz invariant amplitude $M_{f,i}(E)$ using Eqs. (7)-(10), we need to express each outgoing momentum in Fig. 1 in terms of \mathbf{k} , \hat{p}_{NN} and M_{NN} . This can be done by using the standard Lorentz transformation. For a given \mathbf{k} , M_{NN} , and the angles $\Omega_{\mathbf{p}_{NN}}$, we can calculate them by

$$p_{NN} = |\mathbf{p}_{NN}| = \sqrt{\frac{1}{4} M_{NN}^2 - m_N^2}, \quad (19)$$

$$\mathbf{p}_1 = \mathbf{p}_{NN} + \gamma \left(\frac{\gamma}{1 + \gamma} \boldsymbol{\beta} \cdot \mathbf{p}_{NN} - E_N(\mathbf{p}_{NN}) \right) \boldsymbol{\beta}, \quad (20)$$

$$\mathbf{p}_2 = \mathbf{p}_{NN} - \mathbf{p}_1, \quad (21)$$

with

$$\mathbf{P}_{NN} = \mathbf{q} - \mathbf{k} , \quad (22)$$

$$\boldsymbol{\beta} = -\frac{\mathbf{P}_{NN}}{[M_{NN}^2 + \mathbf{P}_{NN}^2]^{1/2}} , \quad (23)$$

$$\gamma = \frac{1}{\sqrt{1 - \boldsymbol{\beta}^2}} . \quad (24)$$

We will also present results of the differential cross section in the the CM frame of the γ - d system. We find that

$$\frac{d\sigma}{d\Omega_c} \equiv \frac{d\sigma}{d\Omega_{\mathbf{k}_c}} = \frac{1}{6} \sum_{\lambda, s_d} \frac{d\sigma(\lambda, s_d)}{d\Omega_{\mathbf{k}_c}} , \quad (25)$$

where

$$\frac{d\sigma(\lambda, s_d)}{d\Omega_{\mathbf{k}_c}} = \int dM_{NN} \frac{d\sigma(\lambda, s_d)}{d\Omega_{\mathbf{k}_c} dM_{NN}} , \quad (26)$$

with

$$\frac{d\sigma(\lambda, s_d)}{d\Omega_{\mathbf{k}_c} dM_{NN}} = \sum_{s_1, s_2} \frac{1}{|\mathbf{v}_{\text{rel},c}|} \frac{(2\pi)^4}{4\omega_c} \frac{1}{2E_d(\mathbf{q}_c)} \int d\Omega_{\mathbf{p}_{NN}} \frac{p_{NN} k_c m_N^2}{E_c} |M_{f,i}(E_c)|^2 , \quad (27)$$

where (ω_c, \mathbf{q}_c) and E_c can be obtained from (ω, \mathbf{q}) and E in the laboratory frame by the Lorentz transformation with $\boldsymbol{\beta} = \mathbf{q}/(\omega + m_d)$. The momentum variables for the calculations of the invariant amplitudes using Eqs. (7)-(10) can be obtained from the same Eqs. (19)-(24), but setting $\mathbf{P}_{NN} = -\mathbf{k}_c$.

We will also present results for three polarization observables of current interest. We choose the z -axis along the incident photon direction, $\mathbf{q} = (q_x, q_y, q_z) = (0, 0, q)$, and the y -axis along the vector product, $\hat{q} \times \hat{k}$. Then, the photon asymmetry Σ for the $d(\gamma, \pi)NN$ reaction is defined by

$$\Sigma_{\gamma d} = \frac{d\sigma(\lambda = 2) - d\sigma(\lambda = 1)}{d\sigma(\lambda = 2) + d\sigma(\lambda = 1)} , \quad (28)$$

where $d\sigma(\lambda)$ denotes either of differential cross sections of Eqs. (16) or (25), but the initial photon polarization is fixed to λ instead of the average. The components $\lambda = 1, 2$ for the linear photon polarization in Eq. (28) are

$$\boldsymbol{\epsilon}_{\lambda=1} = (1, 0, 0) , \quad \boldsymbol{\epsilon}_{\lambda=2} = (0, 1, 0) . \quad (29)$$

The asymmetry E of the circularly polarized photons on a deuteron target polarized along the z -axis ($s_d = +1$) is defined by

$$E_{\gamma d} = \frac{d\sigma(\lambda = 3, s_d = +1) - d\sigma(\lambda = 4, s_d = +1)}{d\sigma(\lambda = 3, s_d = +1) + d\sigma(\lambda = 4, s_d = +1)} , \quad (30)$$

where $d\sigma(\lambda, s_d = +1)$ denotes either of differential cross sections of Eqs. (17) or (26); the deuteron spin orientation is $s_d = +1$ and the components $\lambda = 3, 4$ for the circular photon polarization are defined as

$$\boldsymbol{\epsilon}_{\lambda=3} = \frac{+1}{\sqrt{2}}(1, -i, 0) , \quad \boldsymbol{\epsilon}_{\lambda=4} = \frac{-1}{\sqrt{2}}(1, i, 0) . \quad (31)$$

The asymmetry G of the linearly polarized photons on a polarized deuteron is defined by

$$G_{\gamma d} = \frac{d\sigma(\lambda = 5, s_d = +1) - d\sigma(\lambda = 6, s_d = +1)}{d\sigma(\lambda = 5, s_d = +1) + d\sigma(\lambda = 6, s_d = +1)}, \quad (32)$$

where the components $\lambda = 5, 6$ for the photon polarization are

$$\epsilon_{\lambda=5} = \frac{1}{\sqrt{2}}(1, 1, 0), \quad \epsilon_{\lambda=6} = \frac{1}{\sqrt{2}}(1, -1, 0). \quad (33)$$

III. RESULTS

In our calculations of the amplitudes Eqs. (8)-(10), the $\gamma N, \pi N \rightarrow \pi N$ partial-wave amplitudes up to and including $L = 5$ (L : the πN orbital angular momentum) generated from the ANL-Osaka model of Refs. [19, 20] are taken into account. To calculate the loop-integrations in Eqs. (9) and (10) for the N - and π -exchange mechanisms, respectively, the off-energy-shell two-body matrix elements are generated from solving the scattering equation Eq. (5) for the meson-nucleon scattering and a similar Lippmann-Schwinger equation of Eq. (A8) for the NN scattering. The $NN \rightarrow NN$ partial wave amplitudes up to and including $J = 3$ (J : the NN total angular momentum) generated from the CD-Bonn potential are included in the calculations.

We first compare our predictions with the available data of $d(\gamma, \pi^0)pn$ and $d(\gamma, \pi^-)pp$ reactions. We then examine whether our results can be improved if the employed $\gamma N \rightarrow \pi N$ model of Ref. [20] is adjusted to also fit the recent Mainz data [23, 24] of $\gamma n \rightarrow \pi^0 n$. We also examine the roles of the off-energy-shell and FSI effects in explaining the data. The differences with the approach of Refs. [25, 26] will also be discussed.

A. Comparisons with data of $d(\gamma, \pi)NN$ reactions

We have found that our predictions agree reasonably well with the available data of $d(\gamma, \pi^0)pn$ and $d(\gamma, \pi^-)pp$ reactions. In Figs. 2 and 3, we show some typical comparisons of the data for unpolarized differential cross sections and our results (blue dotted curves) using the amplitudes generated from the ANL-Osaka model. Clearly there are some discrepancies with the data, in particular for $d(\gamma, \pi^0)np$ in the $E_\gamma = 500$ – 750 MeV region (E_γ is the photon energy in the laboratory frame). One possible source of the discrepancies is that, when determining the parameters for the ANL-Osaka model, we used rather scarce $\gamma n \rightarrow \pi^0 n$ dataset that are extracted from $d(\gamma, \pi^0)np$ data. To see whether this is the case, we have extended the fit of Ref. [20] to also include recently extracted data for $\gamma n \rightarrow \pi^0 n$ from Mainz [23, 24], and also recent data for $\gamma n \rightarrow \pi^- p$ from JLab [21, 22]. However, the amount of these new data are much less than the total number of the world data for $\pi N, \gamma N \rightarrow \pi N, \eta N, K\Lambda, K\Sigma$ included in the fit [19, 20] for the ANL-Osaka model. We thus do not expect that the resonance parameters and the hadronic parameters determined in Ref. [20] will be changed significantly by including the recent $\gamma n \rightarrow \pi N$ data, and therefore vary only the parameters for the bare $\gamma n \rightarrow N^*$ couplings in the new fit.

To be consistent with the procedure in constructing the ANL-Osaka model, the calculations for the fits include $L = 0 - 10$ partial waves. In addition to the data of $\pi p, \gamma p \rightarrow \pi N, \eta N, K\Lambda, K\Sigma$ and $\gamma n \rightarrow \pi^0 n, \pi^- p$ included in the fits in Ref. [20], the recent data [21–24] of the unpolarized differential cross sections and E for $\gamma n \rightarrow \pi^0 n, \pi^- p$ are included in the

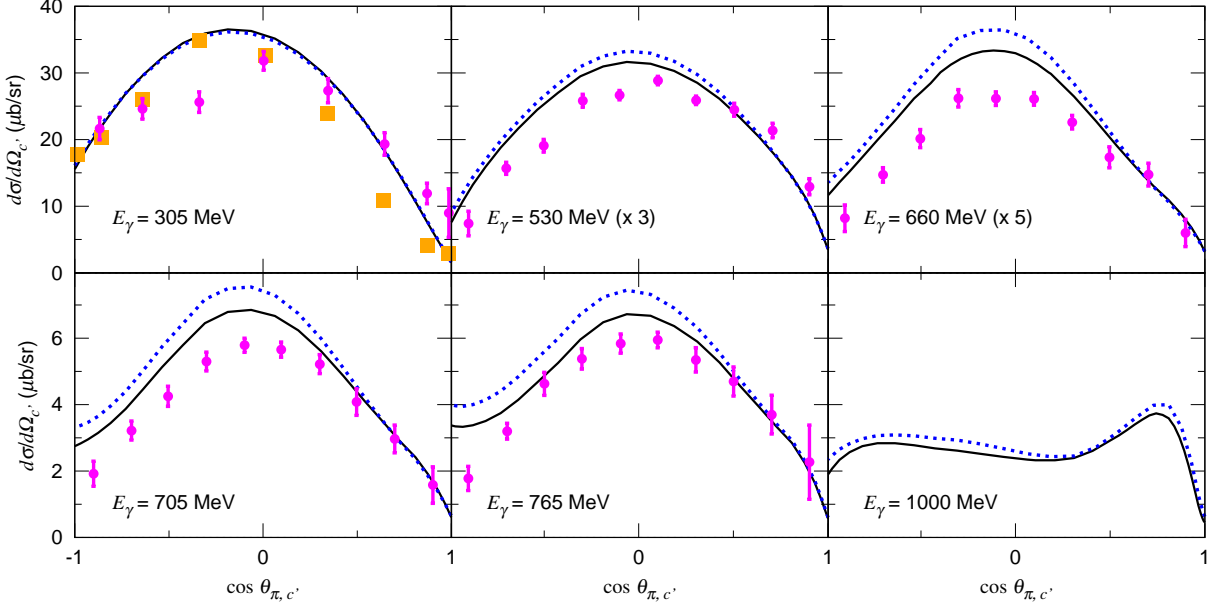


FIG. 2. Differential cross sections for $d(\gamma, \pi^0)pn$ calculated with the $\gamma N \rightarrow \pi N$ amplitudes from the AO model [19, 20] (blue dotted curves) and the new fits including the recent Mainz data [23, 24] of $\gamma n \rightarrow \pi^0 n$ (black solid curves). The cross sections are scaled by the factor in the parenthesis when it is given. The pion emission angle $\theta_{\pi, c'}$ is defined in the frame where the photon momentum $\mathbf{q}_{c'}$ and the deuteron momentum $\mathbf{p}_{d, c'}$ are related by $\mathbf{p}_{d, c'} = -2\mathbf{q}_{c'}$. The photon energies indicated in the panels (E_γ) are those in the laboratory frame. Data are from Ref. [43] (magenta circles) and Ref. [44] (orange squares).

new fits. In Fig. 4, we show the comparisons of our results with the data of the differential cross sections. The fits to the data which are not shown in Fig. 4 are of similar quality and hence are omitted to simplify the presentation. Clearly, the results from this new fit (red solid curves) and those from the ANL-Osaka model (blue dashed curves) are very similar. On the other hand, we see in Fig. 5 some large differences between the fits and the data for the polarization observable E . Further improvements are possible only if we also vary the non-resonant parameters around the values determined in Ref. [20]. This will be worthwhile to pursue when the data for other spin observables, such as G and Σ , become available. For our present purposes, the quality of the fit shown in Figs. 4-5 is sufficiently good. We note here that the higher partial waves ($L = 6 - 10$), which include only non-resonant Born amplitudes, just slightly change the shape of the angular distributions for $\gamma n \rightarrow \pi^- p$ in the forward pion kinematics, and has little effects on $\gamma n \rightarrow \pi^0 n$. These weak higher partial wave amplitudes are therefore neglected in all of our calculations for the $d(\gamma, \pi)NN$ reactions.

With the parameters from the new fits, the calculated differential cross sections for $d(\gamma, \pi^0)pn$ and $d(\gamma, \pi^-)pp$ are the solid curves in Figs. 2 and 3. Comparing with the blue dotted curves from using the ANL-Osaka amplitudes, we see that the agreements with the data for $d(\gamma, \pi^0)pn$ in the region $E_\gamma = 500 - 700$ MeV are improved, but some significant discrepancies with the data remain. It could be due to the neglect of higher order terms in our multiple scattering calculations such as ρ -, σ -, and Δ -exchange terms. On the other hand, we must examine critically the procedures used in extracting the $\gamma n \rightarrow \pi^0 n, \pi^- p$ cross

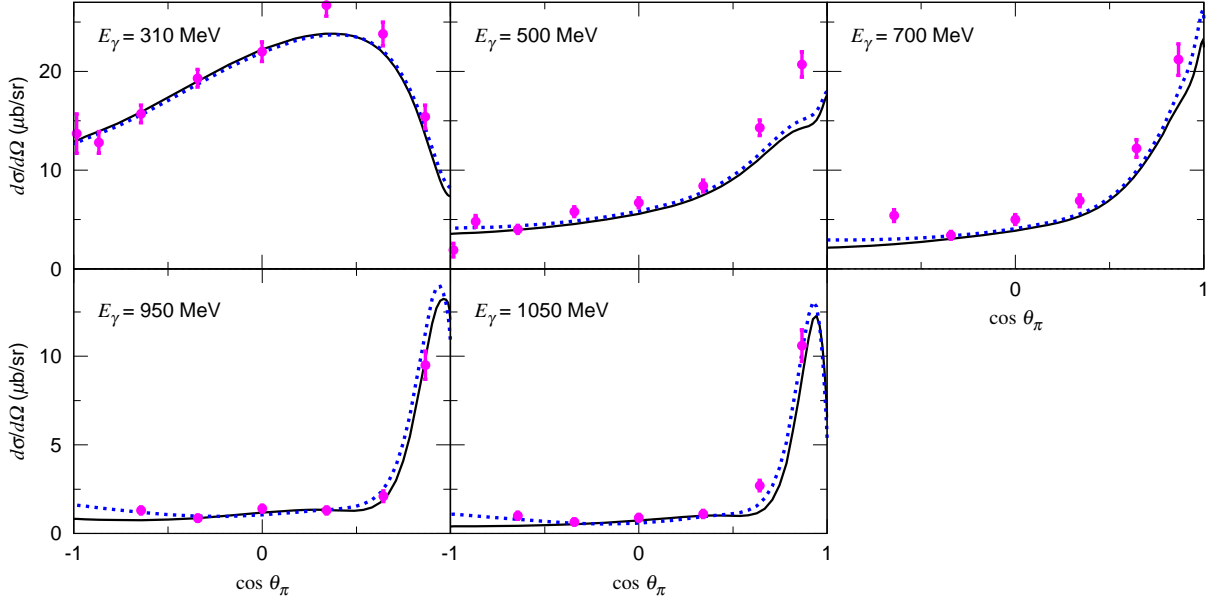


FIG. 3. Differential cross sections for $d(\gamma, \pi^-)pp$ in the laboratory frame. Data are from Ref. [45]. The other features are the same as those in Fig. 2.

sections from the data of $d(\gamma, \pi)NN$. The results presented in the rest of this paper are from using the parameters from the new fit.

B. Off-shell effects

In Sec. II, we show that the two-body matrix elements in the calculations of $d(\gamma, \pi)NN$ amplitudes can be off-energy-shell within the Hamiltonian formulation where all particles are on their mass-shell. In Fig. 6, we see that, if we set all two-body matrix elements in Eqs. (8)–(10) to their on-shell values, the full results (solid curves) are changed to the blue dashed curves. In general, the effects are more significant at low energies and less at higher energies, as illustrated at energies near 300 and 700 MeV in Fig. 6. The differences between the solid and blue dashed curves suggest that the $\gamma n \rightarrow \pi^- p$ extracted using the on-shell calculation results of Refs. [25] are reasonable, but could be modified if the off-shell effects are included in their formulation. The off-shell effects are however model dependent and one must use well-established physics to determine them. In our approach, the off-shell effects are determined by the meson-exchange mechanisms in the ANL-Osaka model and CD-Bonn NN potential. Similar considerations must also be taken in other approaches.

If we further keep only the on-shell pole terms of the propagators by setting

$$\frac{1}{E - E_N(\mathbf{p}_1) - E_N(\mathbf{p}_2) - E_\pi(\mathbf{k}) + i\epsilon} \rightarrow -i\pi\delta(E - E_N(\mathbf{p}_1) - E_N(\mathbf{p}_2) - E_\pi(\mathbf{k})) , \quad (34)$$

in the loop integrations in Eqs. (9) and (10), we obtain the green dotted curves. Clearly, they are significantly different from the solid curves of the full calculations including the off-shell effects, in particular, at $E_\gamma = 305$ MeV for $d(\gamma, \pi^0)pn$, and in the forward angles ($\cos \theta_{\pi,c} \rightarrow 1$) at $E_\gamma = 700$ MeV for $d(\gamma, \pi^-)pp$. Here we mention that Eq. (34) is sometimes

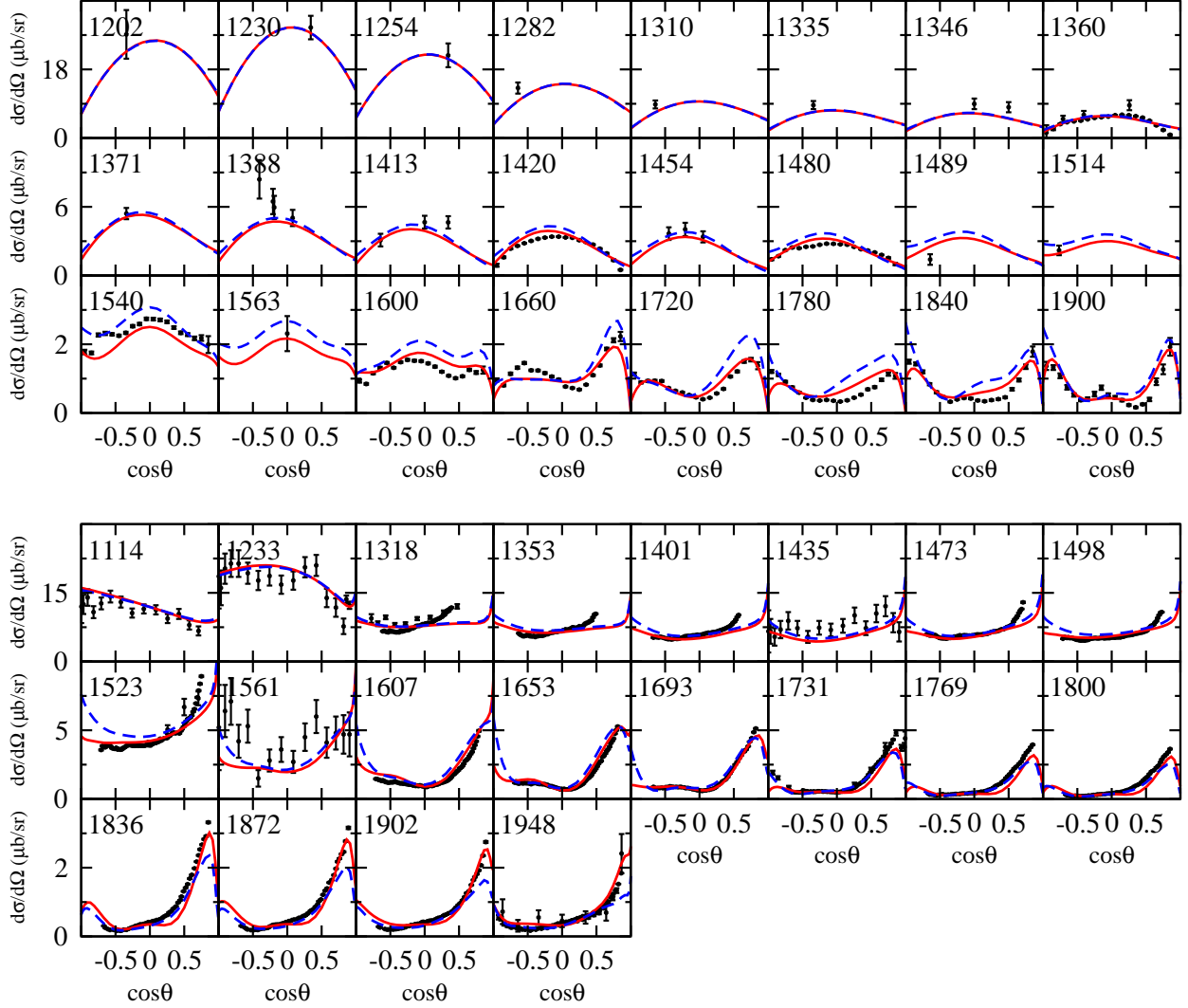


FIG. 4. Differential cross sections for $\gamma n \rightarrow \pi^0 n$ (upper panel) and for $\gamma n \rightarrow \pi^- p$ (lower panel) in the CM frame. The number in each of the panels is the total energy in unit of MeV. The red solid curves are from the new fit while the blue dashed curves are from the AO model [20]. The data are from Ref. [23] for $\gamma n \rightarrow \pi^0 n$ and Ref. [22] for $\gamma n \rightarrow \pi^- p$ in addition to those from the database of the INS DAC Services [46].

used to reduce the computation effort for the loop-integration. The differences between the solid and dotted curves in Fig. 6 give some estimates on the accuracy of such a simplified approach which neglects the off-shell effects completely.

C. Final state interaction effects

In all of the previous investigations of $d(\gamma, \pi^0)pn$ reaction, the N -exchange term illustrated in Fig. 1(b) is found to dominant the FSI. This can be examined by using Eq. (27) to calculate the dependence of the differential cross sections on the NN invariant mass M_{NN} . In the upper half of Fig. 7, we see at a small angle of 10° that the main contributions to

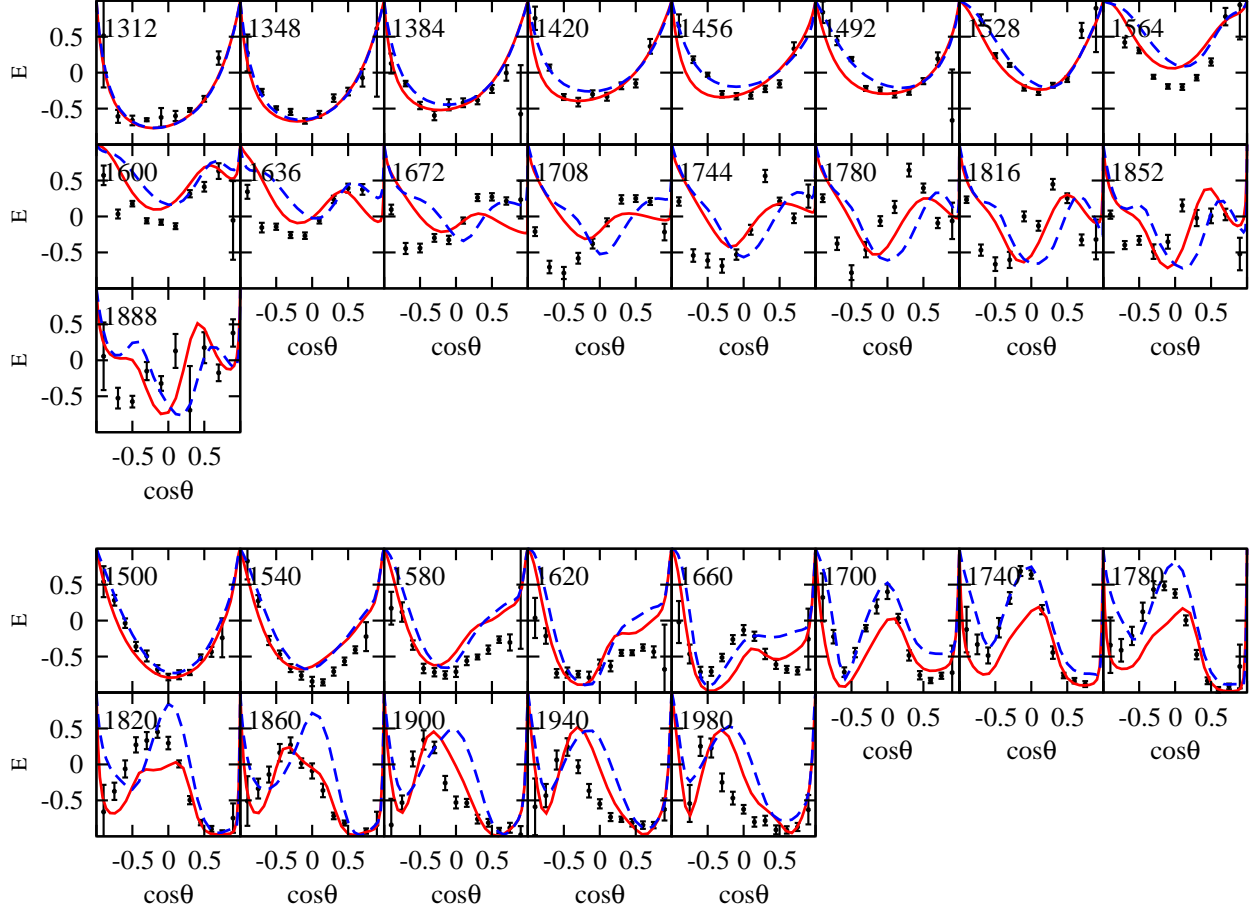


FIG. 5. The polarization observable E for $\gamma n \rightarrow \pi^0 n$ (upper panel) and $\gamma n \rightarrow \pi^- p$ (lower panel). The data are from Ref. [24] for $\gamma n \rightarrow \pi^0 n$ and Ref. [21] for $\gamma n \rightarrow \pi^- p$. The other features are the same as those in Fig. 4.

the differential cross sections of $d(\gamma, \pi^0)pn$ at $E_\gamma = 305$ MeV are in the region close to the NN threshold ($M_{NN} - 2m_N \sim 0$) where the NN scattering is dominated by the ${}^3S_1 + {}^3D_1$ partial wave which is orthogonal to the deuteron bound state. Consequently, the NN FSI greatly reduces the cross section of the impulse (t^{imp}) term (dashed curve) to that of the $t^{\text{imp}} + t^{N\text{-exc}}$ terms (dotted curve). When the pion-exchange term ($t^{\pi\text{-exc}}$) is included, we obtain the solid curve which is almost indistinguishable from the dotted curve. As the scattering angle increases to 60° , the peak position of the M_{NN} spectrum is shifted to the larger invariant mass region where the reduction due to the NN FSI is still large, but much less than that in the forward angles. The FSI effects become weak at large angles 100° and 150° since the large portion of the NN spectrum is in the region far away from the NN threshold.

At a higher photon energy of $E_\gamma = 705$ MeV (lower half of Fig. 7), the reduction due to the NN FSI is similarly dependent on how close the M_{NN} spectrum peak is to the NN threshold. We also note that while the πN FSI effect is much smaller than the NN FSI effect overall, it can give a main FSI correction at large pion emission angles; for example, see the results at $\theta_{\pi,c} \sim 150^\circ$ in the lower half of Fig. 7. Integrating over M_{NN} , the FSI

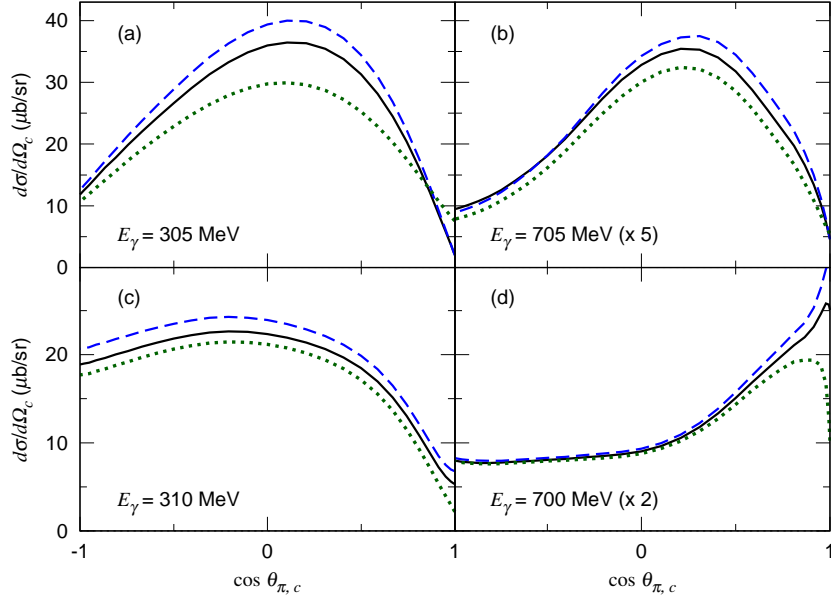


FIG. 6. The off-shell effects on differential cross sections for $d(\gamma, \pi^0)pn$ (a,b) and $d(\gamma, \pi^-)pp$ (c,d) in the CM frame. The photon energy and the scaling factor are indicated in each figure. Solid curves: full calculations; dashed curves: the $\gamma N \rightarrow \pi N$, $NN \rightarrow NN$, and $\pi N \rightarrow \pi N$ amplitudes are put on-shell; dotted curves: only pole terms are kept in loop integrations [see Eq. (34)].

effects on the differential cross sections of $d(\gamma, \pi^0)pn$ are shown in Fig. 8. The large reduction due to the NN FSI is clear. Clearly, the large reduction due to FSI is essential in obtaining a reasonable agreement with the data in Fig. 2. (Note that the results in Fig. 2 is given in a different frame chosen in Ref. [43] to present the data). This is similar to the previous findings [26, 29, 30]. The FSI effects at higher energies are weaker, but still significant in the forward angle, $\theta_{\pi,c} \sim 0^\circ$.

The FSI effects on $d(\gamma, \pi^-)pp$ are shown in Fig. 9. Here, we see that the FSI effect is also clearly visible in the small angle region where the M_{NN} spectrum peak is close to the NN threshold and hence the NN FSI going to the 1S_0 NN partial wave gives a dominant portion of the FSI effect. Contrary to the $d(\gamma, \pi^0)pn$ case, its interference with the impulse term is to enhance the cross section from the dashed curves to the dotted curves. The πN FSI effect is also weak here, as can be seen in the negligible difference between the solid and dotted curves. As the angle increases, the πN FSI effect is getting discernible but overall the FSI effect quickly becomes much smaller. Therefore, the FSI effect on the differential cross sections are very weak, as seen in Fig. 10.

We have also investigated the FSI effects on the polarization observables Σ , E , and G defined in Eqs. (28)-(32) which are of current interests. The results are shown in Figs. 11 and 12. Clearly, the FSI effects do not play an important role here. It will be interesting to compare our predictions with the data in near future.

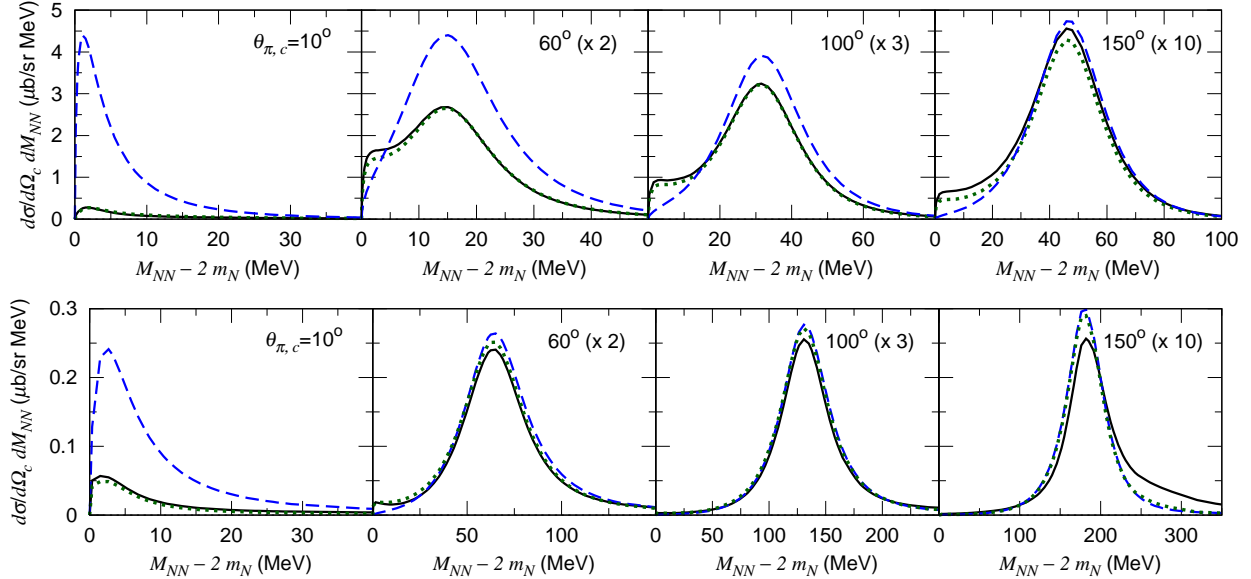


FIG. 7. The NN invariant mass distribution for $d(\gamma, \pi^0)pn$ at $E_\gamma = 305$ MeV (upper row) and $E_\gamma = 705$ MeV (lower row). The pion emission angle in the CM frame along with the scaling factor is indicated in each figure. Dashed curves: impulse; dotted curves: impulse + N -exchange; solid curves: impulse + N -exchange + π -exchange.

IV. SUMMARY

We have applied the ANL-Osaka amplitudes to investigate the $d(\gamma, \pi)NN$ in the nucleon resonance region. Within the multiple scattering formulation, the calculations include the impulse term and the final-state interaction terms due to the pion-exchange and nucleon-exchange mechanisms. The predicted differential cross sections are in good agreement with most of the available data of $d(\gamma, \pi^0)np$ and $d(\gamma, \pi^-)pp$ reactions.

We have shown that the off-shell effects, calculated from the meson-exchange mechanisms, on the propagations of the exchanged nucleon and pion are significant in determining the reaction amplitudes. The FSI effects on the predicted cross sections are found to be important at energies near the $\Delta(1232)$ resonance, and are still significant at higher energies. To complete this investigation, we need to examine the extent to which the predictions presented in this work will be changed when the Δ -, ρ - and σ -exchange mechanisms, which can also be predicted by using the ANL-Osaka amplitudes, are included in our calculations.

ACKNOWLEDGMENTS

We thank W.N. Polyzou for his assistance to the use of their relativistic reaction theory. This work is in part supported by Fundação de Amparo à Pesquisa do Estado de São Paulo (FAPESP), Process No. 2016/15618-8, by JSPS KAKENHI Grant Numbers 25105010, 16K05354, and 18K03632, and by the U.S. Department of Energy, Office of Science, Office of Nuclear Physics, Contract No. DE-AC02-06CH11357. Numerical computations in this work were carried out with SR16000 at YITP in Kyoto University, the High Performance

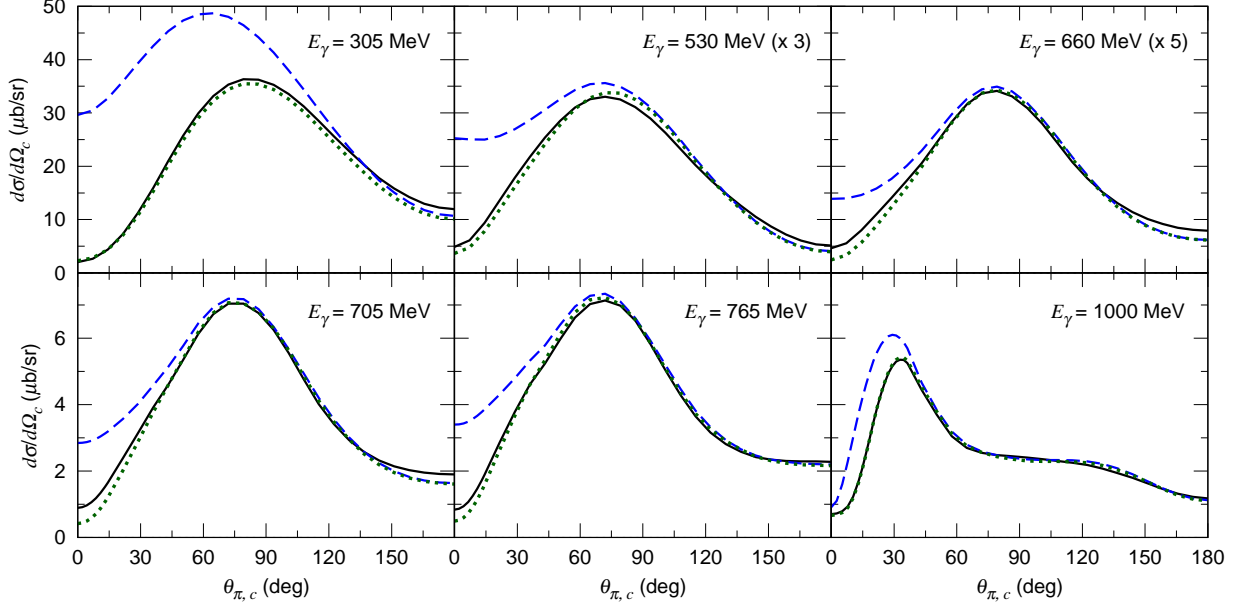


FIG. 8. Differential cross sections for $d(\gamma, \pi^0)pn$ in the CM frame. The reaction mechanisms included in the calculations for each of the curves are the same as those in Fig. 7.

Computing system at RCNP in Osaka University, the National Energy Research Scientific Computing Center, which is supported by the Office of Science of the U.S. Department of Energy under Contract No. DE-AC02-05CH11231, and the use of the Bebop [or Blues] cluster in the Laboratory Computing Resource Center at Argonne National Laboratory.

Appendix A: Ingredients for $\gamma d \rightarrow \pi N_1 N_2$ matrix elements in Eqs. (8)-(10)

The off-energy-shell two-body matrix elements for calculating Eqs. (8)-(10) are defined in the γ - d laboratory frame. Here we give formulas for getting these matrix elements from the matrix elements in the CM frame of γN , πN , and NN systems. Our formula are derived from using the procedures of Refs. [37, 38] within the instant form of relativistic quantum mechanics [39]. The details of this approach can be found in these references. Here we only give the formulas used in our numerical calculations.

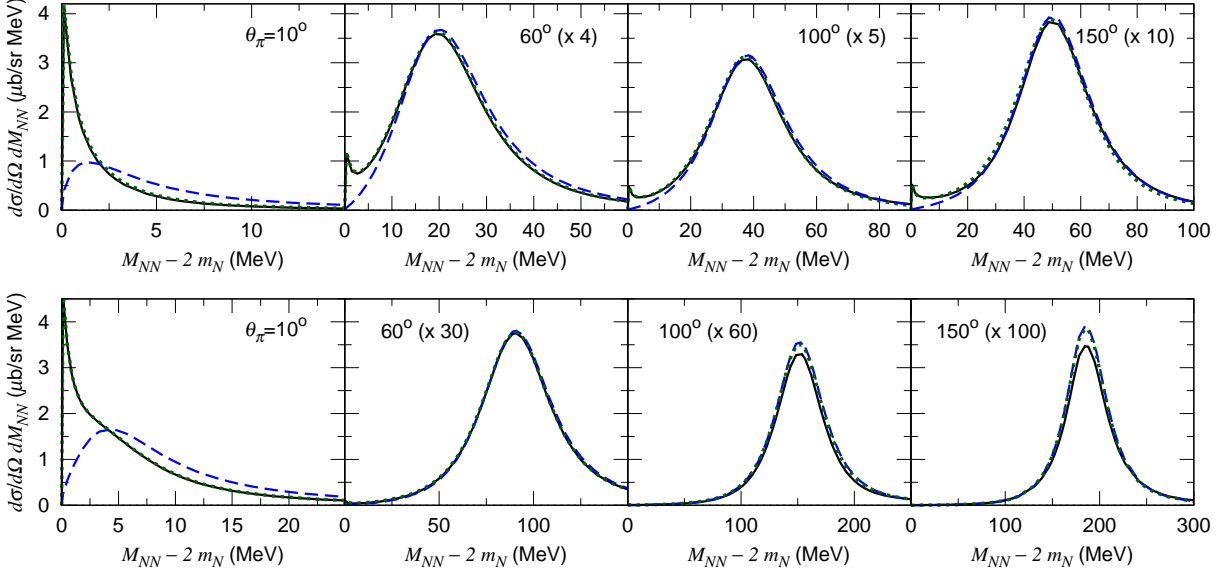


FIG. 9. The NN invariant mass distribution for $d(\gamma, \pi^-)pp$ at $E_\gamma = 310$ MeV (upper row) and $E_\gamma = 700$ MeV (lower row). The pion emission angles indicated in the figures are those in the laboratory frame. The reaction mechanisms included in the calculations for each of the curves are the same as those in Fig. 7.

1. $\gamma N \rightarrow \pi N'$ matrix elements

The off-shell $\gamma N \rightarrow \pi N'$ matrix element $\langle \pi N' | t_{\pi N, \gamma N}(W) | \gamma N \rangle$ in Eqs. (8)-(10), is related to those evaluated in the CM frame of $\pi N'$ by

$$\begin{aligned}
& \langle \pi(\mathbf{k}, t_\pi) N'(\mathbf{p}', s', t') | t_{\pi N, \gamma N}(W) | \gamma(\mathbf{q}, \lambda) N(\mathbf{p}, s, t) \rangle \\
&= \langle \pi(\mathbf{k}, t_\pi) N'(\mathbf{p}', s', t') | \epsilon_\lambda^\mu(q) [j(W)]_\mu | N(\mathbf{p}, s, t) \rangle \\
&= \sqrt{\frac{|\mathbf{q}_{\bar{c}}| E_\pi(\mathbf{k}_{\bar{c}}) E_N(-\mathbf{q}_{\bar{c}}) E_N(-\mathbf{k}_{\bar{c}})}{|\mathbf{q}| E_\pi(\mathbf{k}) E_N(\mathbf{p}) E_N(\mathbf{p}')}} \sum_{\mu\nu} \epsilon_\lambda^\mu(q) \Lambda_\mu^\nu(p_t) \sum_{s_{\bar{c}}, s'_{\bar{c}}} R_{s'_{\bar{c}}, s'}^*(p', p_t) R_{s_{\bar{c}}, s}(p, p_t) \\
&\times \langle \pi(\mathbf{k}_{\bar{c}}, t_\pi) N'(-\mathbf{k}_{\bar{c}}, s'_{\bar{c}}, t') | [j_{\bar{c}}(W)]_\nu | N(-\mathbf{q}_{\bar{c}}, s_{\bar{c}}, t) \rangle, \tag{A1}
\end{aligned}$$

where the suffixes ' \bar{c} ' indicate quantities in the CM system of $\pi N'$, $\epsilon_\lambda^\mu(q)$ is the photon polarization vector, $j_\mu(W)$ is the current operator, $p_t = p' + k$ is a four-momentum defined by $\mathbf{p}_t = \mathbf{p}' + \mathbf{k}$ and $p_t^0 = E_N(\mathbf{p}') + E_\pi(\mathbf{k})$. The CM matrix elements of the current operator, $\langle \pi(\mathbf{k}_{\bar{c}}, t_\pi) N'(-\mathbf{k}_{\bar{c}}, s'_{\bar{c}}, t') | [j_{\bar{c}}(W)]_\mu | N(-\mathbf{q}_{\bar{c}}, s_{\bar{c}}, t) \rangle$, from the ANL-Osaka model are calculated following the procedure detailed in Appendix D of Ref. [19], and their normalization is specified by Eq. (D2) of the reference.

In Eq. (A1), the quantity $\Lambda_\mu^\nu(p_t)$ boosts the CM momenta $a_{\bar{c}} = (k_{\bar{c}}^0, \mathbf{k}_{\bar{c}}) [(q_{\bar{c}}^0, \mathbf{q}_{\bar{c}})]$ to the Lab momenta $a_L = (k^0, \mathbf{k}) [(q^0, \mathbf{q})]$ by the Lorentz transformation,

$$\begin{aligned}
a_L^0 &= \sum_\nu \Lambda_\nu^0(p_t) a_{\bar{c}}^\nu = \frac{a_{\bar{c}}^0 p_t^0 + \mathbf{p}_t \cdot \mathbf{a}_{\bar{c}}}{m_t}, \\
a_L^i &= \sum_\nu \Lambda_\nu^i(p_t) a_{\bar{c}}^\nu = a_{\bar{c}}^i + p_t^i \left[\frac{\mathbf{p}_t \cdot \mathbf{a}_{\bar{c}}}{m_t(m_t + p_t^0)} + \frac{a_{\bar{c}}^0}{m_t} \right], \tag{A2}
\end{aligned}$$

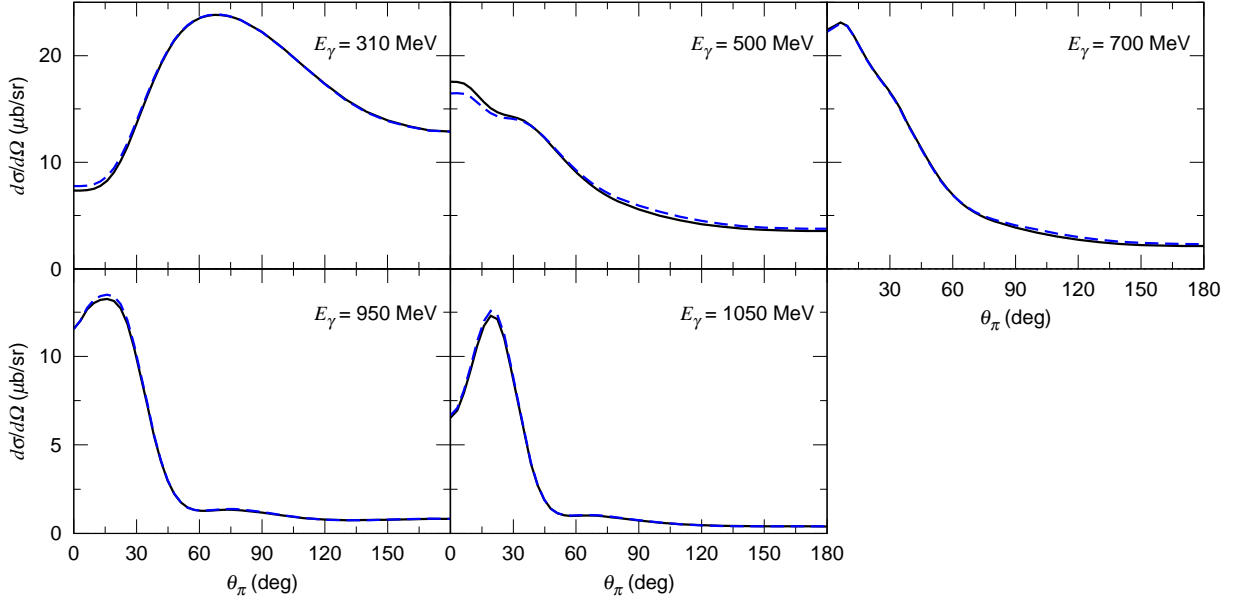


FIG. 10. Differential cross sections for $d(\gamma, \pi^-)pp$ in the laboratory frame. The reaction mechanisms included in the calculations for each of the curves are the same as those in Fig. 7.

where the index $i = 1, 2, 3$ is a spatial component and $m_t \equiv \sqrt{\mathbf{p}_t \cdot \mathbf{p}_t}$.

The spin rotation matrix $R_{s_{\bar{c}},s}(p, p_t)$ in Eq. (A1) is given [37, 38] explicitly as:

$$R_{s_{\bar{c}},s}(p, p_t) = \langle s_{\bar{c}} | B^{-1}(p_{\bar{c}}/m_N) B^{-1}(p_t/m_t) B(p/m_N) | s \rangle, \quad (\text{A3})$$

where $|s_{\bar{c}}\rangle$ is the spin state of the nucleon, $p_{\bar{c}}$ is obtained from the nucleon momentum p in the laboratory frame by the Lorentz transformation of Eq. (A2), and

$$\begin{aligned} B(p/m) &= \frac{1}{\sqrt{2m(p^0 + m)}} ((p^0 + m)\mathbb{1} + \mathbf{p} \cdot \boldsymbol{\sigma}), \\ B^{-1}(p/m) &= \frac{1}{\sqrt{2m(p^0 + m)}} ((p^0 + m)\mathbb{1} - \mathbf{p} \cdot \boldsymbol{\sigma}), \end{aligned} \quad (\text{A4})$$

where $\boldsymbol{\sigma}$ is the Pauli operator and $\mathbb{1}$ is the unit matrix.

2. $\pi'N' \rightarrow \pi N$ matrix element

The half-off-shell $\pi'N' \rightarrow \pi N$ scattering amplitudes in the laboratory frame, appearing in Eq. (10), are related to those in the πN CM frame by

$$\begin{aligned} & \langle \pi(\mathbf{k}, t_\pi) N(\mathbf{p}, s, t) | t_{\pi N}(M_{\pi N}) | \pi'(\mathbf{k}', t'_\pi) N'(\mathbf{p}', s', t') \rangle \\ &= \sqrt{\frac{E_\pi(\mathbf{k}_{\bar{c}}) E_N(-\mathbf{k}_{\bar{c}}) E_\pi(\mathbf{k}'_{\bar{c}}) E_N(-\mathbf{k}'_{\bar{c}})}{E_\pi(\mathbf{k}) E_N(\mathbf{p}) E_\pi(\mathbf{k}') E_N(\mathbf{p}')}} \sum_{s_{\bar{c}}, s'_{\bar{c}}} R_{s_{\bar{c}},s}^*(p, p_t) R_{s'_{\bar{c}},s'}(p', p_t) \\ & \times \langle \pi(\mathbf{k}_{\bar{c}}, t_\pi) N(-\mathbf{k}_{\bar{c}}, s_{\bar{c}}, t) | t_{\pi N}^{\bar{c}}(M_{\pi N}) | \pi'(\mathbf{k}'_{\bar{c}}, t'_\pi) N'(-\mathbf{k}'_{\bar{c}}, s'_{\bar{c}}, t') \rangle, \end{aligned} \quad (\text{A5})$$

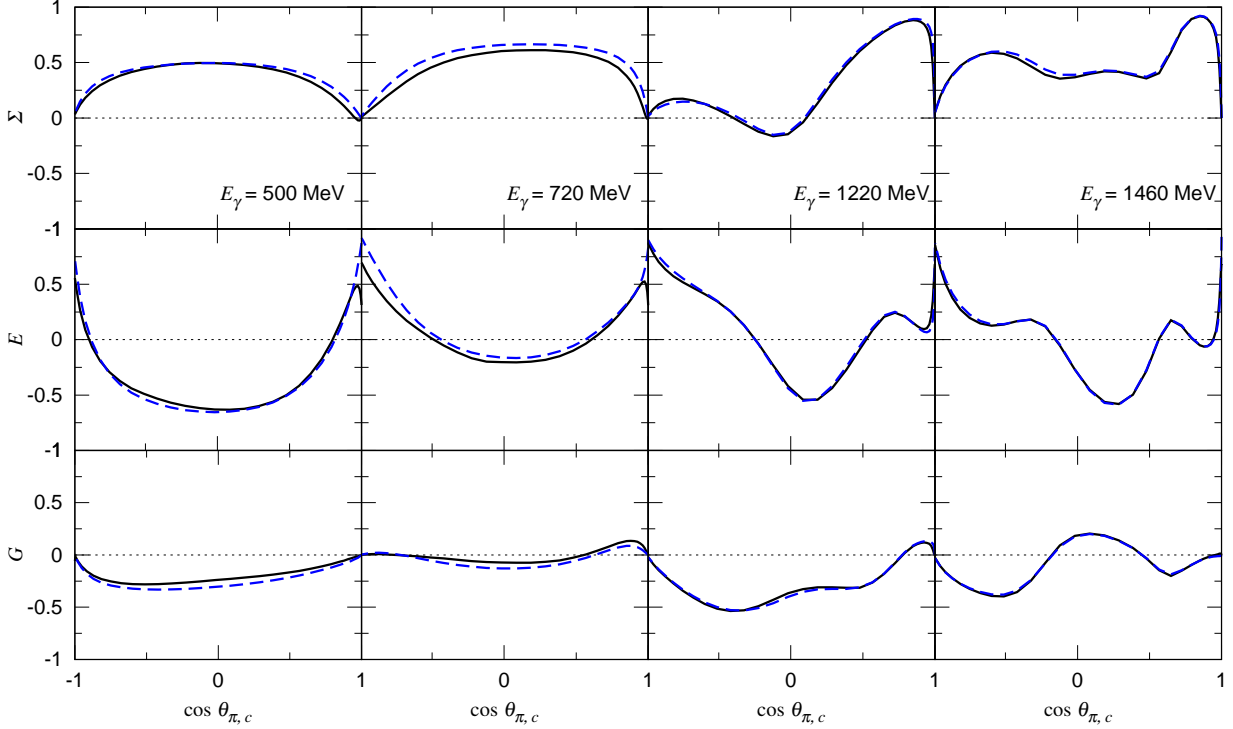


FIG. 11. The polarization observables Σ , E , and G for $d(\gamma, \pi^0)pn$ in the CM frame. Dashed curves: impulse; solid curves: impulse + N -exchange + π -exchange.

where the momentum $\mathbf{k}_{\bar{c}}$ in the πN CM frame is related to \mathbf{k} in the laboratory frame by the Lorentz transformation Eq. (A2). Here we choose $\mathbf{p}_t = \mathbf{k} + \mathbf{p}$ and $p_t^0 = E_\pi(\mathbf{k}) + E_N(\mathbf{p})$. Within our formulation where an energy of a particle x is always related to its off-shell momentum (\mathbf{p}_x) by $E_x = \sqrt{|\mathbf{p}_x|^2 + m_x^2}$, the same Lorentz transformation does not bring the off-shell $\pi'N'$ system in the laboratory frame into their CM frame. Therefore, we define the $\pi'N'$ relative momentum in the πN CM frame by $\mathbf{k}'_{\bar{c}} = (m_N \tilde{\mathbf{k}}'_{\bar{c}} - m_\pi \tilde{\mathbf{p}}'_{\bar{c}})/(m_N + m_\pi)$, where $\tilde{\mathbf{k}}'_{\bar{c}}$ and $\tilde{\mathbf{p}}'_{\bar{c}}$ are related to \mathbf{k}' and \mathbf{p}' by the same Lorentz transformation Eq. (A2). The πN scattering amplitudes in the πN CM frame, $\langle \pi(\mathbf{k}_{\bar{c}}, t_\pi) N(-\mathbf{k}_{\bar{c}}, s_{\bar{c}}, t) | t_{\pi N}^{\bar{c}}(M_{\pi N}) | \pi'(\mathbf{k}'_{\bar{c}}, t'_\pi) N'(-\mathbf{k}'_{\bar{c}}, s'_{\bar{c}}, t') \rangle$, are calculated following the procedure detailed in Appendix C of Ref. [19], and their normalization is specified by Eq. (C7) of the reference.

3. $N'_1 N'_2 \rightarrow N_1 N_2$ matrix element

The half off-shell $N'_1 N'_2 \rightarrow N_1 N_2$ matrix elements in the laboratory frame, appearing in Eq. (9), are related to those in the $N_1 N_2$ CM frame by

$$\begin{aligned}
& \langle N_1(\mathbf{p}_1, s_1, t_1) N_2(\mathbf{p}_2, s_2, t_2) | T_{NN}(M_{N_1 N_2}) | N'_1(\mathbf{p}'_1, s'_1, t_1) N'_2(\mathbf{p}'_2, s'_2, t_2) \rangle \\
&= \sqrt{\frac{E_N^2(\mathbf{p}_{\bar{c}}) E_N^2(\mathbf{p}'_{\bar{c}})}{E_N(\mathbf{p}_1) E_N(\mathbf{p}_2) E_N(\mathbf{p}'_1) E_N(\mathbf{p}'_2)}} \sum_{s_{1\bar{c}}, s_{2\bar{c}}, s'_{1\bar{c}}, s'_{2\bar{c}}} R_{s_{1\bar{c}}, s_1}^*(p_1, p_t) R_{s_{2\bar{c}}, s_2}^*(p_2, p_t) R_{s'_{1\bar{c}}, s'_1}(p'_1, p_t) R_{s'_{2\bar{c}}, s'_2}(p'_2, p_t) \\
&\times \langle N_1(\mathbf{p}_{\bar{c}}, s_{1\bar{c}}, t_1) N_2(-\mathbf{p}_{\bar{c}}, s_{2\bar{c}}, t_2) | T_{NN}^{\bar{c}}(M_{N_1 N_2}) | N'_1(\mathbf{p}'_{\bar{c}}, s'_{1\bar{c}}, t_1) N'_2(-\mathbf{p}'_{\bar{c}}, s'_{2\bar{c}}, t_2) \rangle, \quad (\text{A6})
\end{aligned}$$

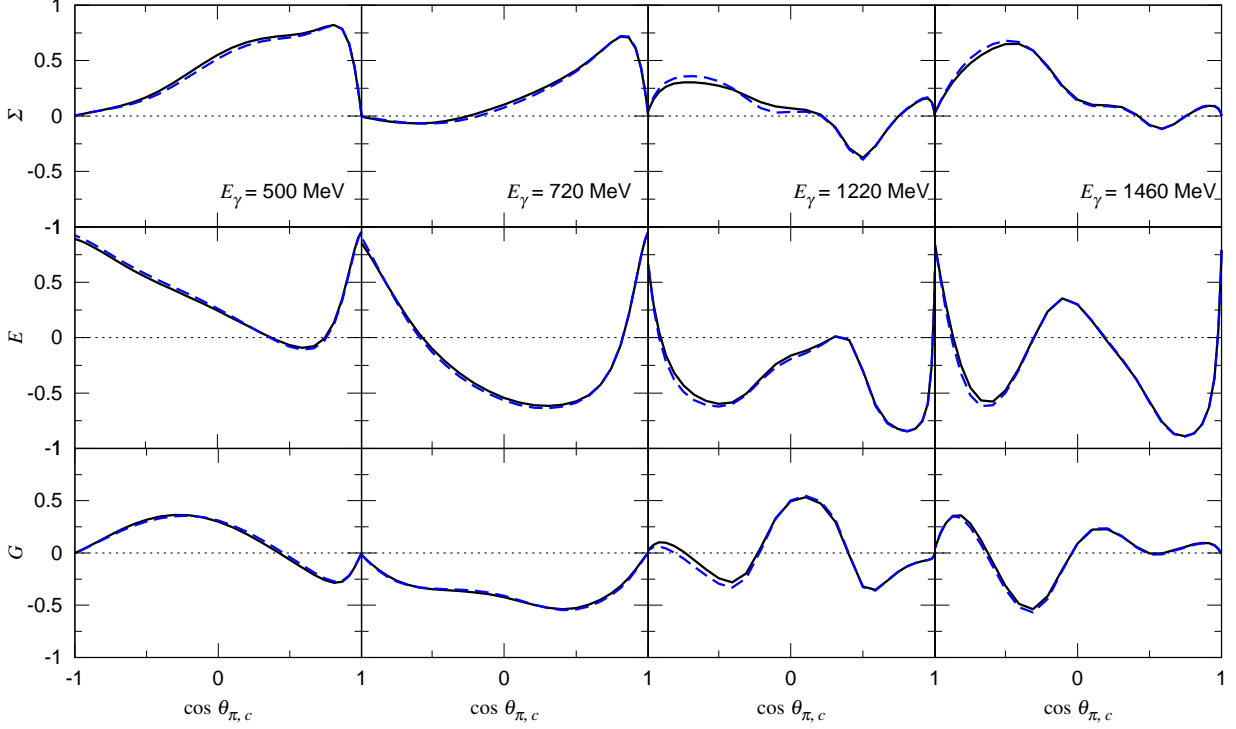


FIG. 12. The polarization observables Σ , E , and G for $d(\gamma, \pi^-)pp$ in the CM frame. The other features are the same as those in Fig. 11.

with p_t being $\mathbf{p}_t = \mathbf{p}_1 + \mathbf{p}_2$ and $p_t^0 = E_N(\mathbf{p}_1) + E_N(\mathbf{p}_2)$. Regarding the NN relative momenta, we use the non-relativistic relation $\mathbf{p}_{\bar{c}} = (\mathbf{p}_1 - \mathbf{p}_2)/2$ and $\mathbf{p}'_{\bar{c}} = (\mathbf{p}'_1 - \mathbf{p}'_2)/2$. The NN T -matrix $\langle T_{NN}^{\bar{c}} \rangle$ is expanded in terms of partial waves as

$$\begin{aligned}
& \langle N_1(\mathbf{p}_{\bar{c}}, s_{1\bar{c}}, t_1) N_2(-\mathbf{p}_{\bar{c}}, s_{2\bar{c}}, t_2) | T_{NN}^{\bar{c}}(M_{N_1 N_2}) | N'_1(\mathbf{p}'_{\bar{c}}, s'_{1\bar{c}}, t_1) N'_2(-\mathbf{p}'_{\bar{c}}, s'_{2\bar{c}}, t_2) \rangle \\
&= \sum_{JLL'ST} \left(\frac{1 - (-1)^{L+S+T}}{2^{|t_1+t_2|}} \right) \sum_{S^z S'^z L^z L'^z J^z T^z} t_{NN}^{JLL'ST}(|\mathbf{p}_{\bar{c}}|, |\mathbf{p}'_{\bar{c}}|; M_{N_1 N_2}) \\
&\times (1/2, t_1, 1/2, t_2 | TT^z) (1/2, s_{1\bar{c}}, 1/2, s_{2\bar{c}} | SS^z) (LL^z SS^z | JJ^z) Y_{LL^z}(\hat{p}_{\bar{c}}) \\
&\times (1/2, t_1, 1/2, t_2 | TT^z) (1/2, s'_{1\bar{c}}, 1/2, s'_{2\bar{c}} | SS'^z) (L'L'^z SS'^z | JJ^z) Y_{L'L'^z}^*(\hat{p}'_{\bar{c}}), \quad (A7)
\end{aligned}$$

where $t_{NN}^{JLL'ST}$ is a partial wave NN amplitude characterized by the quantum numbers $JLL'ST$ meaning of which are self-evident in the above equation. On- and off-shell partial wave NN amplitudes are obtained by solving the following Lippmann-Schwinger equation:

$$t_{NN}^{JLL'ST}(p, p'; M_{N_1 N_2}) = v_{NN}^{JLL'ST}(p, p') + \sum_{L''} \int_0^\infty q^2 dq \frac{v_{NN}^{JLL''ST}(p, q) t_{NN}^{JL''L'ST}(q, p'; M_{N_1 N_2})}{M_{N_1 N_2} - 2m_N - \frac{q^2}{m_N} + i\epsilon}, \quad (A8)$$

where we use the CD-Bonn potential [34] for $v_{NN}^{JLL'ST}(p', p)$.

4. Deuteron wave function

The deuteron wave function in its rest frame, appearing in Eqs. (8)-(10), is more explicitly written as

$$\langle N_1(\mathbf{p}, s_1, t_1) N_2(-\mathbf{p}, s_2, t_2) | \Psi_d(s_d) \rangle = \left[\frac{\delta_{s, s_d}}{\sqrt{4\pi}} u_s(p) + (2, s_d - s, 1, s | 1s_d) u_d(p) Y_{2, s_d - s}(\hat{p}) \right] \times (1/2, s_1, 1/2, s_2 | 1s)(1/2, t_1, 1/2, t_2 | 00), \quad (\text{A9})$$

with $s = s_1 + s_2$. The radial s - and d -wave functions, denoted by u_s and u_d respectively, are normalized as $\int_0^\infty dp p^2 (|u_s(p)|^2 + |u_d(p)|^2) = 1$. We use the CD-Bonn potential [34] to generate the deuteron wave function. The nucleon momentum distribution in the deuteron is given by

$$\rho_d(p) = |u_s(p)|^2 + |u_d(p)|^2. \quad (\text{A10})$$

-
- [1] H. Kamano, T.-S. H. Lee, S.X. Nakamura, and T. Sato, <http://www.phy.anl.gov/theory/research/anl-osaka-pwa/>
 - [2] See review by R. Machleidt in *Advance in Nuclear Physics*, edited by J.W. Negele and E. Vogt (Pleum, New York, 1989), Chap.2 Vol. 19.
 - [3] See review by A. Donnachie in *High Energy Physics*, edited by E. Burhop (Academic Press, New York, 1972), Vol.5, P.1.
 - [4] See review by S. Capstick and W. Robert, *Prog. Part. Nucl. Phys.* **45**, S241-S331 (2000).
 - [5] T. Sato and T.-S.H. Lee, *Phys. Rev. C* **54**, 2660 (1996); **63**, 055201 (2001).
 - [6] A. Matsuyama, T. Sato, and T.-S.H. Lee, *Phys. Rept* **439**, 193 (2007).
 - [7] L. Alvarez-Ruso, Y. Hayato, and J. Nieves, *New J. Phys.* **16**, 075015 (2014); S.X. Nakamura et al., *Rept. Prog. Phys.* **80**, 056301 (2017); L. Alvarez-Ruso et al., arXiv:1706.03621 [hep-ph].
 - [8] B. Julia-Diaz, T.-S.H. Lee, A. Matsuyama, and T. Sato, *Phys. Rev. C* **76**, 065201 (2007).
 - [9] B. Julia-Diaz, T.-S.H. Lee, A. Matsuyama, T. Sato, and L.C. Smith, *Phys. Rev. C* **77**, 045201 (2008).
 - [10] J. Durand, B. Julia-Diaz, T.-S.H. Lee, B. Saghai, and T. Sato, *Phys. Rev. C* **78**, 025204 (2008).
 - [11] N. Suzuki, T. Sato, and T.-S.H. Lee, *Phys. Rev. C* **79**, 025205 (2009).
 - [12] H. Kamano, B. Julia-Diaz, T.-S.H. Lee, A. Matsuyama, T. Sato, *Phys. Rev. C* **79**, 025206 (2009).
 - [13] B. Julia-Diaz, H. Kamano, T.-S.H. Lee, A. Matsuyama, T. Sato, and N. Suzuki, *Phys. Rev. C* **80**, 025207 (2009).
 - [14] H. Kamano, B. Julia-Diaz, T.-S.H. Lee, A. Matsuyama, T. Sato, *Phys. Rev. C* **80**, 065203 (2009).
 - [15] N. Suzuki, B. Julia-Diaz, H. Kamano, T.-S.H. Lee, A. Matsuyama, and T. Sato, *Phys. Rev. Lett.* **104**, 042302 (2010).
 - [16] H. Kamano, S.X. Nakamura, T.-S.H. Lee, and T. Sato, *Phys. Rev. C* **81**, 065207 (2010).
 - [17] N. Suzuki, T. Sato, and T.-S.H. Lee, *Phys. Rev. C* **82**, 045206 (2010).
 - [18] A. Sandorfi, S. Hoblit, H. Kamano, and T.-S.H. Lee, *J. Phys. G* **38**, 053001 (2011).
 - [19] H. Kamano, S.X. Nakamura, T.-S.H. Lee, and T. Sato, *Phys.Rev. C* **88**, 035209 (2013).

- [20] H. Kamano, S.X. Nakamura, T.-S.H. Lee, and T. Sato, Phys. Rev. C **94**, 015201 (2016).
- [21] D. Ho et al. (CLAS Collaboration), Phys. Rev. Lett. **118**, 242002 (2017).
- [22] P.T. Mattione et al. (CLAS Collaboration), Phys. Rev. C **96**, 035204 (2017).
- [23] M. Dieterle et al. (A2 Collaboration), Phys. Rev. Lett. **112**, 142001 (2014).
- [24] M. Dieterle et al., Phys. Lett. **B770**, 523 (2017).
- [25] V.E. Tarasov, W.J. Briscoe, H. Gao, A.E. Kudryavtsev, and I.I. Strakovsky, Phys. Rev. C **84**, 035203 (2011).
- [26] V.E. Tarasov, W.J. Briscoe, M. Dieterle, B. Krusche, A.E. Kudryavtsev, M. Ostrick, and I.I. Strakovsky, Phys. Atom. Nucl. **79**, 216 (2016).
- [27] T. Sato, M. Kobayashi, and H. Ohtsubo, Prog. Theor. Phys. **98**, 927 (1997).
- [28] H. Feshbach, *Theoretical Nuclear Physics, Nuclear Reactions* (Wiley, New York, 1992); A.K. Kerman, H. McManus, and R.M. Thaler, Ann. Phys. **8**, 551 (1959).
- [29] E.M. Darwish, H. Arenhövel and M. Schwamb, Eur. Phys. J. **A16**, 111 (2003).
- [30] A. Fix and H. Arenhövel, Phys. Rev. C **72**, 064005 (2005).
- [31] M.I. Levchuk, A.Yu. Loginov, A.A. Sidorov, V.N. Stibunov and M. Schumacher, Phys. Rev. C **74**, 014004 (2006).
- [32] M. Schwamb, Phys. Rep. **485**, 109 (2010).
- [33] J.-J. Wu, T. Sato, and T.-S.H. Lee, Phys. Rev. C **91**, 035203 (2015).
- [34] R. Machleidt, Phys. Rev. C **63**, 024001 (2001).
- [35] A.W. Thomas and R.H. Landau, Phys. Rept. **58**, 121 (1980).
- [36] T.-S.H. Lee, Phys. Lett **67B**, 282 (1977).
- [37] W.N. Polyzou and Ch. Elster, J. Phys. G **41**, 094006 (2014); W.N. Polyzou, W. Glöckle, and H. Witała, Few Body Syst. **56**, 395 (2015).
- [38] W. N. Polyzou, private communication.
- [39] See review by B.D. Keidster and W.N. Polyzou in *Advance in Nuclear Physics*, by J.W. Negele and E. Vogt (Pleum, New York, 1991), Vol. 20, p.225.
- [40] T.-S.H. Lee, Phys. Rev. Lett. **50**, 1571 (1983); Phys. Rev. C **29**, 195 (1984).
- [41] Review by H. Garcilazo and H.Mizutani, *π -NN System* (World Scientific, Singapore, 1990).
- [42] S.X. Nakamura, H. Kamano, and T. Ishikawa, Phys. Rev. C **96**, 042201(R) (2017).
- [43] B. Krusche et al., Eur. Phys. J. **A6**, 309 (1999).
- [44] U. Siodlaczek et al., Eur. Phys. J. **A10**, 365 (2001).
- [45] P. Benz et al. (Aachen-Bonn-Hamburg-Heidelberg-Muenchen Collaboration), Nucl. Phys. **B65**, 158 (1973).
- [46] CNS Data Analysis Center, George Washington University, <http://gwdac.phys.gwu.edu>